

The Removal of Tunnel Vibration Induced Corruption in Aero-Optical Measurements

Nicholas De Lucca¹, Stanislav Gordeyev², Adam Smith³, Eric Jumper⁴
University of Notre Dame, Notre Dame, IN, 46545

Matthew Whiteley⁵
MZA Associates Corporation, Dayton, OH, 45430

and

Tyler Neale⁶
Arnold Air Force Base, Tullahoma, TN, 37389

Wavefront measurements of a turbulent boundary layer were performed at the University of Notre Dame. Optical access windows to the tunnel were instrumented with 16 accelerometers to measure the tunnel-induced vibrations in the optical windows. A combination of spectral Proper Orthogonal Decomposition (POD) and Linear Stochastic Estimation (LSE) were used to remove vibration induced effects in the wavefronts. Through a combination of Tip/Tilt removal and LSE-POD filtering, a reduction of greater than 85% in OPD_{RMS} was observed. A brief optimization study on accelerometer number requirements showed that even instrumenting each optical access window with a single accelerometer provided substantial improvement in vibration-induced error reduction. Wavefront statistics, including spectra, correlation lengths, and OPD_{RMS} for LSE-POD filtered measurements of a $M = 0.35$ turbulent boundary layer were calculated. The resulting statistics were shown to be in good agreement with previous studies of subsonic turbulent boundary layers.

I. Introduction

In the last 10-15 years, aero-optical research has experienced an increased interest to utilize near-IR lasers on aircraft for either direct energy or free-space communication systems [1]. The resurgence has included substantial experimental work on aero-optical turrets [2,3,4] and boundary layer research [5,6] along with numerous CFD investigations of aero-optical flows, [1,7,8,9] for instance. Obtaining high quality aero-optical measurements can be a challenge that depends on many factors which can be completely unrelated to aero-optical phenomenon. It is desirable to be able to perform high quality aero-optical measurements at a variety of facilities in academia, industry and government and to be able to collect correct aero-optical data and to compare data between facilities.

One of the major factors that can affect aero-optical data quality is tunnel vibrations, as it almost always couples into aero-optical measurements. Excessive tunnel vibration that couples into the beam train introduces significant global beam jitter, and, as a result, beam steering systems such as fast steering mirrors can be required. Jitter effects introduced by mechanical vibration have been studied previously at Notre Dame [10]. Additionally, work has been done to correlate these global jitter effects with higher order wavefront aberrations [11].

¹ Graduate Student, Department of Mechanical and Aerospace Engineering, Hessert Laboratory for Aerospace Research, Notre Dame, IN 46556, AIAA Student Member.

² Research Associate Professor, Department of Mechanical and Aerospace Engineering, Hessert Laboratory for Aerospace Research, Notre Dame, IN 46556, AIAA Associate Fellow.

³ Graduate Student, Department of Mechanical and Aerospace Engineering, Hessert Laboratory for Aerospace Research, Notre Dame, IN 46556, AIAA Student Member.

⁴ Professor, Department of Mechanical and Aerospace Engineering, Hessert Laboratory for Aerospace Research, Notre Dame, IN 46556, AIAA Fellow.

⁵ Vice President, Senior Scientist, 1360 Technology Ct, Ste 200, Dayton, OH 45430, AIAA Member.

⁶ Project Manager, Propulsion Wind Tunnel Ground Test Complex AEDC, Arnold AFB, Tullahoma, TN, 37389

Tunnel vibration can also introduce higher-order effects. The laser beam must propagate through optical windows into and/or from the tunnel, and those optical windows will have specific vibrational modes. If these specific vibrational modes introduce a non-linear wavefront variation over the laser aperture, they will not manifest themselves as jitter effects. This higher-order vibrational effect will vary between experimental facilities as the dominant modes and frequencies depend on the optical window composition, shape and vibrational excitation. Although it has been shown that tunnel vibration effects only dominate for low frequencies, below 1 kHz [10], it is important to properly remove them in a way that preserves any aero-optical information at those frequencies instead of strictly filtering or ignoring data in these ranges. This can enable the extraction of physical phenomenon across a larger range of frequencies. To accomplish the removal of tunnel vibration effects from aero-optical data, this paper proposes a purely statistical technique using a combination of a spectral Proper Orthogonal Decomposition (POD) and a Linear Stochastic Estimation (LSE).

II. Experimental Setup

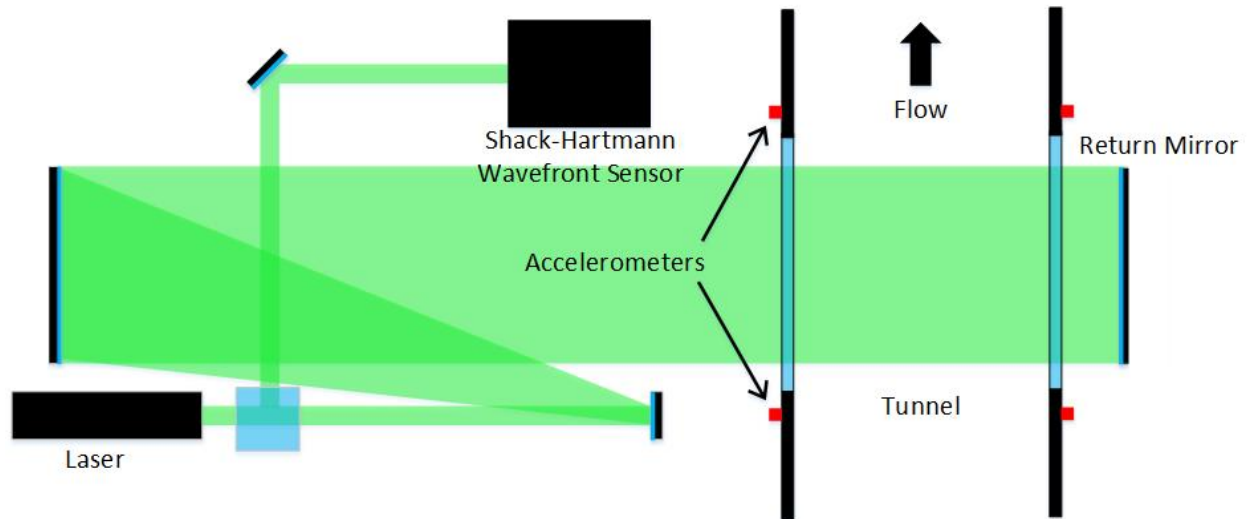


Figure 1: Optical Setup

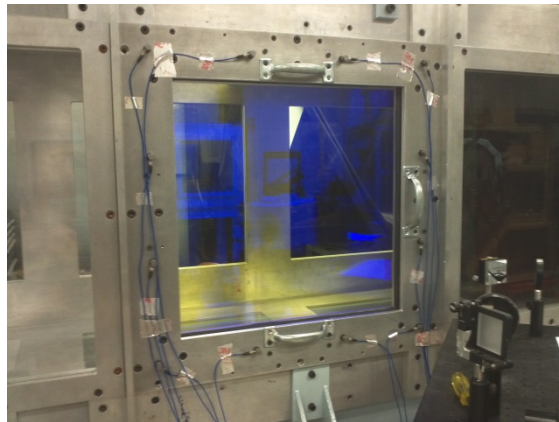


Figure 2: Picture of optical window and accelerometers

Simultaneous aero-optical and mechanical vibrations measurements were performed in White Field Tunnel at the University of Notre Dame, with the test section of 3 ft x 3 ft x 8 ft. Data were collected at Mach numbers of 0.25 and 0.35. To measure the aero-optical aberrations, the laser beam was expanded to 10 inch in diameter and propagated through the test section, normal to the window, as shown in Figure 1. A return mirror on the other side of the test section reflected the beam along exactly the same path it came in. After the returning beam on the optical table was reflected off using a beam splitter, it was contracted to a 12-mm beam. A high speed Shack-Hartmann wavefront sensor was used to obtain time-resolved wavefront sequences. Wavefronts with 10-inch in diameter with

66x66 sub-apertures were acquired at a rate of 5.4 kHz, and an additional set was collected with a reduced spatial resolution of 33x33 sub-apertures sampled at a higher frame rate of 10 kHz.

The windows' vibration was measured using several 1-axis accelerometers attached to window frames along the windows' perimeters. A picture of the accelerometers attached to the tunnel is given in Figure 2, and the accelerometer arrangements are given above in Figure 3. Two different configurations were used. For the first configuration, shown in Figure 3, left, all of the accelerometers were placed on the tunnel side facing the optical table. The spacing between accelerometers was 8 inches. In this configuration, 12 1-axis accelerometers were used. The second configuration, given in Figure 3, left, had 8 accelerometers on each side of the tunnel, spaced equally at 12 inches. A total of 16 one-axis accelerometers were used. The accelerometer data for both cases were obtained at a sample rate equal to five times the wavefront sample rate. This corresponds to 27 kHz for 66x66 wavefront cases and 50 kHz 33x33 cases. The accelerometer data were obtained simultaneously with the wavefront data.

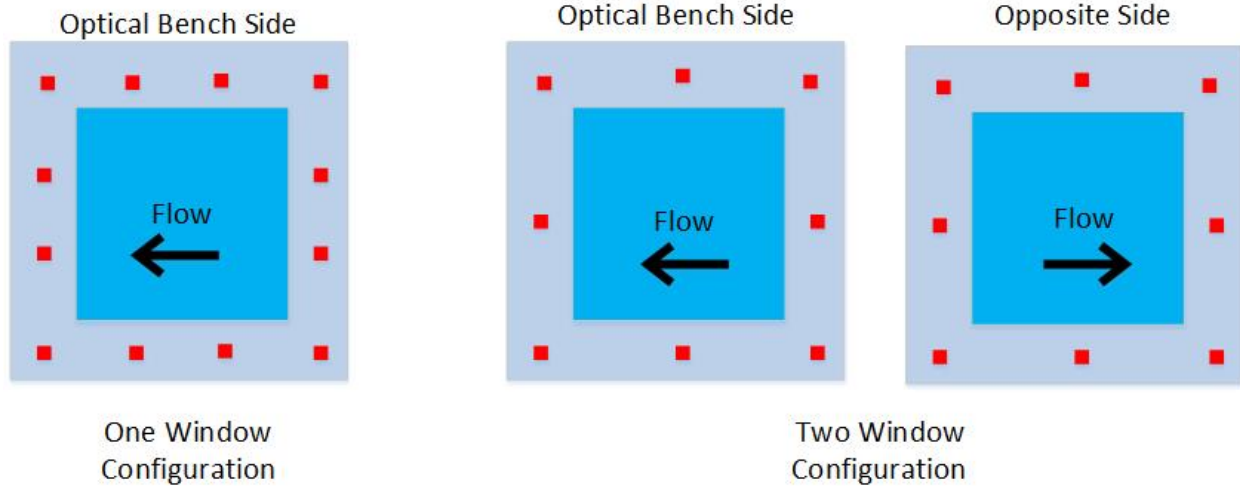


Figure 3: Accelerometer arrangements

III. Spectral LSE-POD Technique

The corruption introduced by the tunnel-induced vibration of the optical windows on the aero-optical data was removed through a combination of spectral POD and LSE. The spectral POD technique is very similar to a traditional POD [12,13,14], but implemented in the spectral domain [15],

$$W(x, y, t) \xrightarrow{FT} \hat{W}(x, y, f)$$

$$\hat{W}(x, y, f) = \sum_n a_n(f) \Phi_n(x, y, f)$$

where POD modes, Φ_n , and the corresponding spectral coefficients, a_n , are calculated from the spectral cross-correlation matrix, S , as,

$$S(x, y; x', y'; f) = \langle \hat{W}^*(x, y, f) \hat{W}(x', y', f) \rangle$$

$$\int S(x, y; x', y'; f) \Phi_n(x', y', f) dx' dy' = \lambda_n(f) \Phi_n(x, y, f)$$

$$a_n(f) = \int \hat{W}(x, y, f) \Phi_n^*(x, y, f) dx dy$$

Eigenvalues, λ_n , are the POD decomposition of the aperture-averaged wavefront spectrum,

$$\sum_n \lambda_n(f) = \left\langle \left| \hat{W}(x, y, f) \right|_{(x,y)}^2 \right\rangle = PSD(f)$$

The spectral POD is advantageous in several ways. As the standard POD provides the fastest-converging set of eigenmodes to describe a system, the spectral POD gives the fastest converging set of modes for describing the behavior at each frequency. So, only few dominant POD modes and their coefficients should be considered, which greatly reduces the computational requirements in the analysis. Further, as mechanical vibrations are typically manifested by several distinct excited frequencies, often only these frequencies should be included in the analysis.

The mechanically-induced component due to mechanical motion of the tunnel windows was estimated and removed using Linear Stochastic Estimation [16], also known as minimum mean-square error (MMSE) estimation. In most general form, the LSE technique approximates a measured signal, x_i , (jitter, wavefronts) using a linear sum of other measurements, y_i , (accelerometers) multiplied by the estimation coefficient matrix, L_{ij} ,

$$x_i^{LSE} = L_{ij}y_j, \text{ where } L_{ij} = \langle x_i y_k \rangle \langle y_j y_k \rangle^{-1}$$

The estimated signal is then subtracted from the original signal to obtain aero-optical-only component. The LSE-technique makes no assumption about the relationship between the measured quantities; it only utilizes the statistical correlation between them. Also, the estimation matrix, L , needs to be solved only once, making the LSE technique computationally-effective. The technique was demonstrated to be effective in removing a vibrationally-induced component from aero-optical jitter [10].

In this paper the LSE technique was applied to the first few dominant spectral POD modes and is called the LSE-POD technique. The procedure was implemented in several steps:

1. Perform Fourier Transformation (FT) of wavefronts (WF) and accelerometer (y_i) channels,

$$W(x, y, t) \xrightarrow{FT} \hat{W}(x, y, f)$$

$$y_i(t) \xrightarrow{FT} \hat{y}_i(f)$$

2. Compute spectral POD modes and coefficients of wavefronts, using first N modes,

$$\hat{W}(x, y, f) \approx \sum_{n=1}^N a_n(f) \Phi_n(x, y, f)$$

3. Use the FT of the accelerometer channels (y_i) and use POD coefficients (a_n) in the LSE technique to compute the L -matrix, $L_i^n(f) = \langle a_n(f) \hat{y}_i^*(f) \rangle / \langle \hat{y}_i(f) \hat{y}_i^*(f) \rangle$. The "expectation" is then taken for each frequency, $a_n^{LSE}(f) = \sum_{\text{all accels}} L_i^n(f) \hat{y}_i(f)$

$$a_n^{LSE}(f) = \sum_{\text{all accels}} L_i^n(f) \hat{y}_i(f)$$

4. Subtract the result of the LSE estimation from the POD spectral coefficients; the residual is the aero-optical spectrum for each mode,

$$a_n^{AO}(f) = a_n(f) - a_n^{LSE}(f)$$

$$\hat{W}^{AO}(x, y, f) = \sum_n a_n^{AO}(f) \Phi_n(x, y, f)$$

5. Recover a filtered wavefront sequence with an inverse FT,

$$\hat{W}^{AO}(x, y, f) \xrightarrow{IFT} W^{AO}(x, y, t)$$

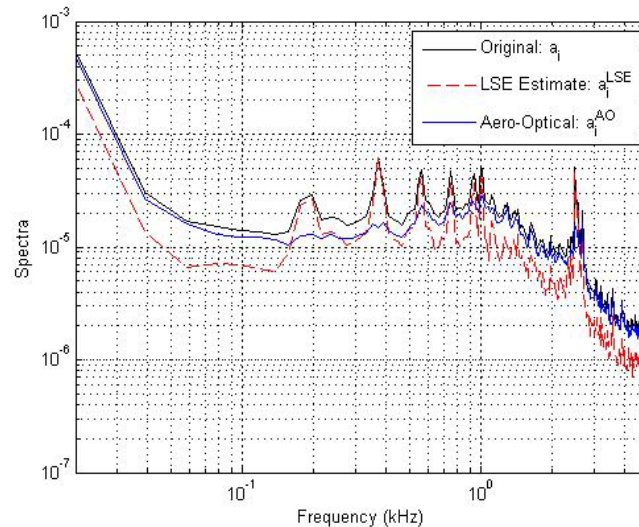


Figure 4: The POD-LSE technique applied to the first POD mode. $M = 0.35$, two-window configuration.

An example of the implementation of this technique for the first POD mode is shown in Figure 4. The original spectrum (a black line) has several distinct peaks around 400, 550, 750, 900, 1000 and 2480 Hz. After estimating the mechanical component (a red line), the resulted aero-optical signal (a blue line), which in this experiment was caused only by turbulent boundary layers on the tunnel walls, has all peaks significantly reduced in amplitude, except for the peak at 2480 Hz; as the peak is un-correlated with the motion of the tunnel windows, it might indicate mechanical vibration of other optical elements on the optical table, for instance.

IV. Results

POD-LSE Filtering Results

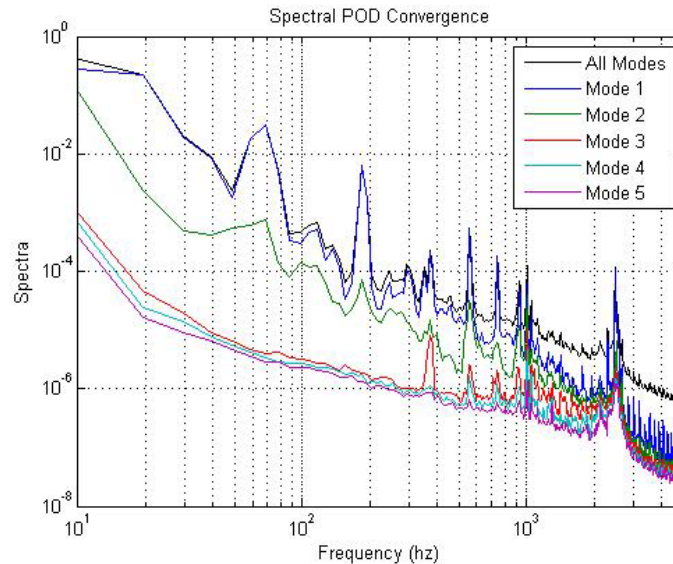


Figure 5: Convergence of first 5 spectral POD modes. $M = 0.35$, two-window configuration.

An example of the spectra of the first five POD modes is shown in Figure 5. At frequencies below 1000 Hz, the spectrum is almost entirely determined by the first two POD modes. This is the range of frequencies that the mechanical vibration is expected to dominate. There are several distinct peaks in the spectrum below 1000 Hz; these peaks are the result of tunnel vibrational modes. As the tunnel vibrates, the optical windows deform and wavefront errors are introduced. These wavefront errors are expected to appear at specific frequencies which correspond to the vibration modes of the windows. These peaks are determined almost entirely by the first two POD modes, with a little contribution from the higher modes. Above 1000 Hz, there is a single peak at 2480 Hz which is also described almost solely by the first two POD modes; this peak is likely a higher frequency vibration mode of the window. Other than the single dominant peak, the first 5 modes do not fully capture the spectral behavior of the wavefronts above 1000 Hz. In this range, boundary layer aero-optical effects begin to dominate. With a 10 inch beam aperture, the structures are also significantly smaller than the aperture size and are spatially uncorrelated across the entire aperture. As a result more POD modes are required to fully characterize the high frequency behavior of the wavefronts.

The spectra of the first 5 modes after tunnel vibration effects are removed are shown in Figure 6, left. The dominant peaks below 1000 Hz are significantly attenuated using the LSE technique, especially for the first two modes, but they are still present in the third mode with less attenuation than is observed in the first two. Outside of the distinct peaks, the LSE removal technique does not substantially affect the magnitude of the spectra. This is shown in Figure 6, right. Below the 185 Hz peak, there is little correlation with the accelerometers, leading to minimal reduction in the spectra using this technique. This range is also dominated by vibration effects, but it is likely that these are vibrational effects that are not measured by the accelerometers, such as vibration of optical components on the table. Except for frequencies above 2.5 kHz, 30 modes were found to be sufficient to fully characterize the wavefront spectra, as they contain 95% of the original signal.

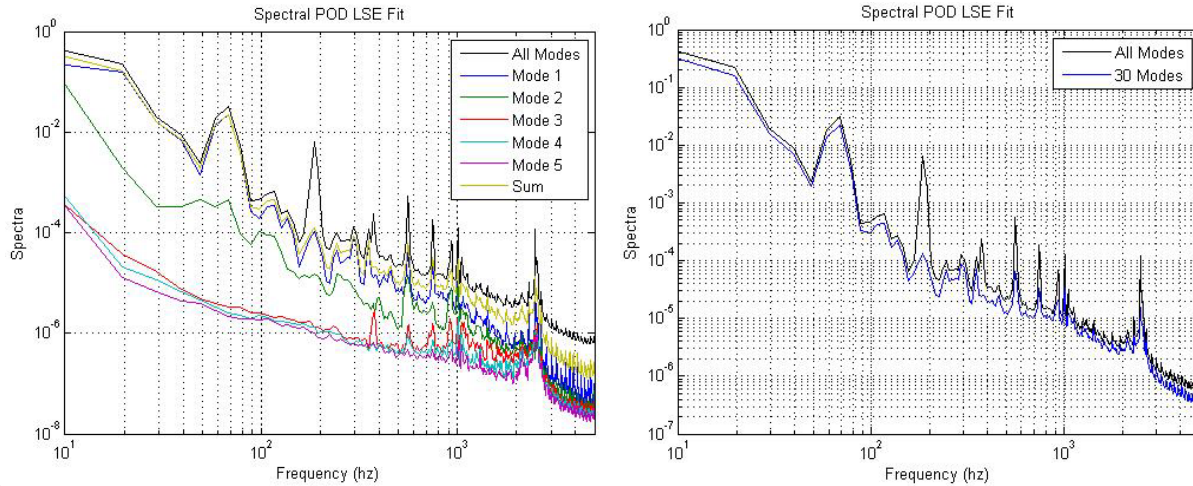


Figure 6: Left: Spectra after tunnel vibration effects are removed through LSE-POD technique. Right: the sum of the first 30 mechanically-related modes, compared to the sum of all mechanically-related modes. $M = 0.35$, two-window configuration.

The maps of the spatial distribution of OPD_{RMS} shown in Figure 7 before (left plot) and after (right plot) applying the LSE-POD technique, demonstrate the magnitude of reduction that can be achieved through filtering out the vibrational effects. The corrected wavefronts, Figure 7 right, were tip/tilt removed, filtered below 126 Hz and corrected via the previously described POD-LSE technique. The original wavefronts, left, show a minimum value of OPD_{RMS} of just under 0.1 microns, up to a maximum value approaching 1 micron around the edges of the aperture. This variation is much larger than the corrected wavefronts, which have fairly uniform spatial distribution of OPD_{RMS} around 0.017 microns. The uniform distribution of OPD_{RMS} is expected for boundary layer flows, as the intensity of the turbulence does not increase substantially over the aperture. Overall, the combined filtering techniques gave a reduction of 85% to greater than 95% depending on the specific aperture location. Also, estimation of boundary-layer effects for this tunnel [5] gives the value of 0.015 microns of OPD_{RMS} , which is very close to the experimentally-extracted value.

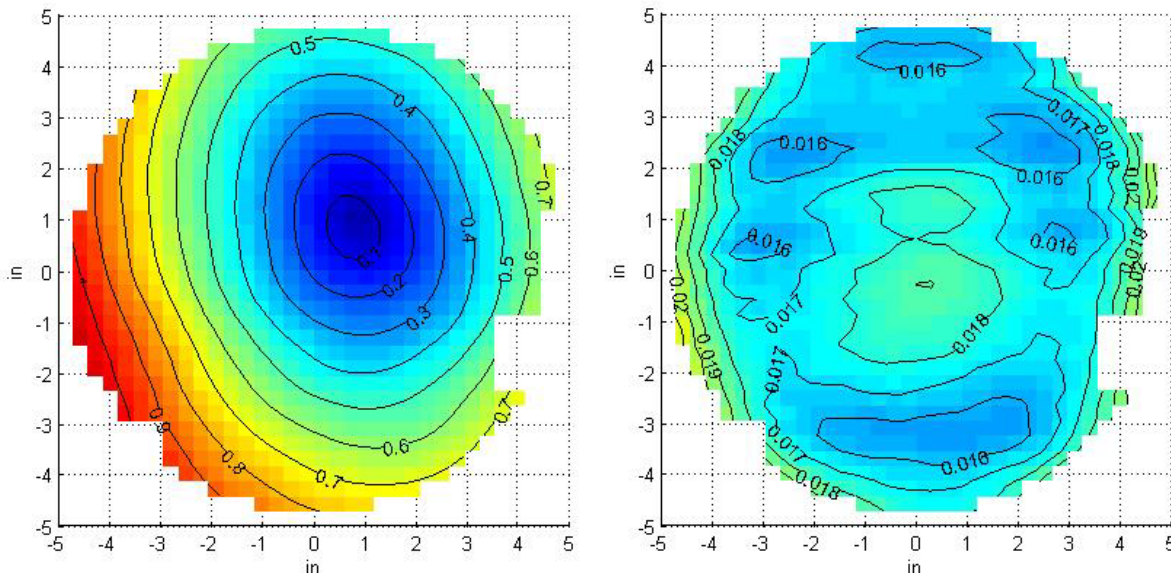


Figure 7: Maps of spatial distribution of OPD_{RMS} for non-tip/tilt removed wavefronts, left and tip/tilt and vibration effect removed wavefronts, right.

Optimization of Accelerometer Locations

In the experiment, 16 accelerometers were used, 8 accelerometers per window, to estimate the mechanical vibration of the tunnel windows. To check the sensitivity of the presented LSE-POD technique to the number and the location of accelerometers per window, additional optimization studies were performed to determine what are optimal locations of a fixed number of accelerometers to provide the most vibration removal from aero-optical data. Since accelerometers on both tunnel windows are needed to estimate mechanical vibrations, only a symmetrical accelerometer placement was considered in the studies. In other words, for any accelerometer on one window, an accelerometer at the same relative location on the opposite window was also included, as schematically shown in Figure 8. Thus, if N accelerometers were placed around one window, the same number of accelerometers were placed symmetrically around the opposite window and, if we define the location of accelerometers on one window, the accelerometer locations on the opposite window are defined automatically.

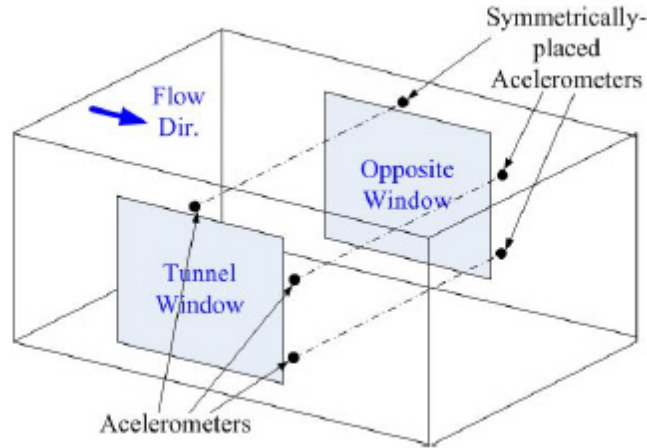


Figure 8: Symmetrical accelerometer placement for Notre Dame tunnel windows.

In the optimization studies we consider 4 cases: with 1 accelerometer per window, 2 accelerometers per window, 4 accelerometers per window and 8 accelerometers per window (the full configuration). For every case, all possible accelerometer placements were considered, the resulting "cleaned" wavefront spectrum was calculated using 30 POD modes, similar to the one shown in Figure 5, and the optimal accelerometer location was identified as the one with the most reduction of vibration-related peaks. The locations are shown in Figure 9. The best locations for accelerometers are along the window edges. The wavefront reconstruction results are shown in Figure 10. The original wavefront spectrum as labeled as a baseline. The reconstructed spectrum shows a monotonic trend in reducing the amplitude of the mechanically-related peaks with increasing number of accelerometers used in the reconstruction. So, for this experiment, technically the more accelerometers are used in the reconstruction, the better is the reconstructed wavefront spectrum. This result probably stems from the relatively large size of the tunnel windows, so many accelerometers are needed to properly measure a complex pattern of mechanical vibration of the window. However, even using 2 accelerometers per window significantly reduced the amplitude of the most of the corrupting peaks. It is expected that for small window 4 accelerometers per window are likely sufficient to significantly remove corrupting peaks from aero-optical spectra.

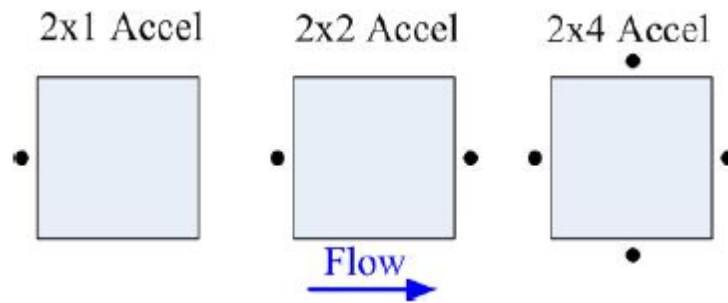


Figure 9: Optimal accelerometer locations for different number of accelerometers.

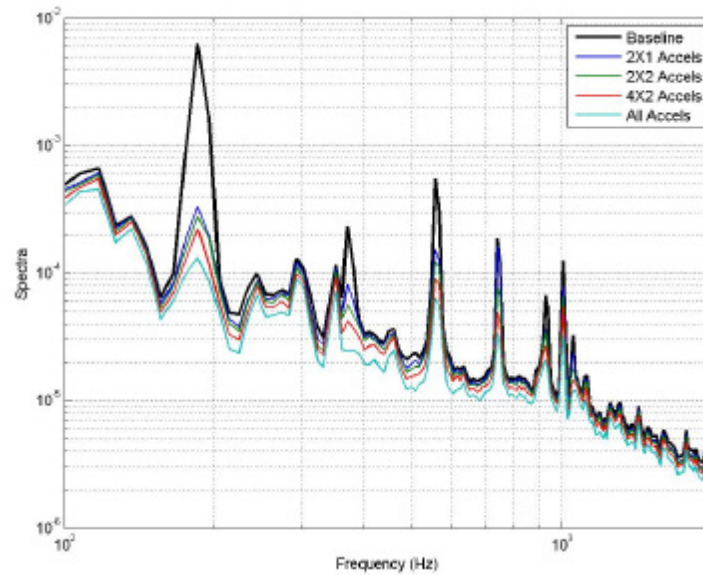


Figure 10: Reconstructed window-averaged wavefront spectrum using LSE-POD technique with 30 POD modes for different number of accelerometers. The original wavefront spectrum is labeled as baseline. $M = 0.35$.

Boundary Layer Results

Time series of filtered wavefronts were reconstructed using the first 30 modes obtained from the LSE-POD technique, and the resulting wavefront statistics were computed and compared to results from previous boundary layer studies. First, measurements of beam deflection angle were obtained using the Shack-Hartmann sensor sampling at 40 kHz (this case used a reduced spanwise lenslet resolution). From this data the deflection angle amplitude spectra, $\hat{\theta}(f)$, was computed and corrected for sub-aperture filtering effects using the expression prescribed in [5]. This spectrum was compared in Figure 11a to the empirical analytical expression for deflection angle spectrum from [5] in order to estimate the thickness, δ , of the measured boundary layer. The empirical expression for deflection angle spectra from [5] showed the best agreement with the spectra from the present study for $\delta = 4.0$ cm, which is in good agreement with estimates of boundary layer thickness from previous boundary layer measurements in this facility [17]. Note that compared to the model from [5], there is significant low-frequency corruption in the measured amplitude spectrum, presumably in this case from wind tunnel vibrations.

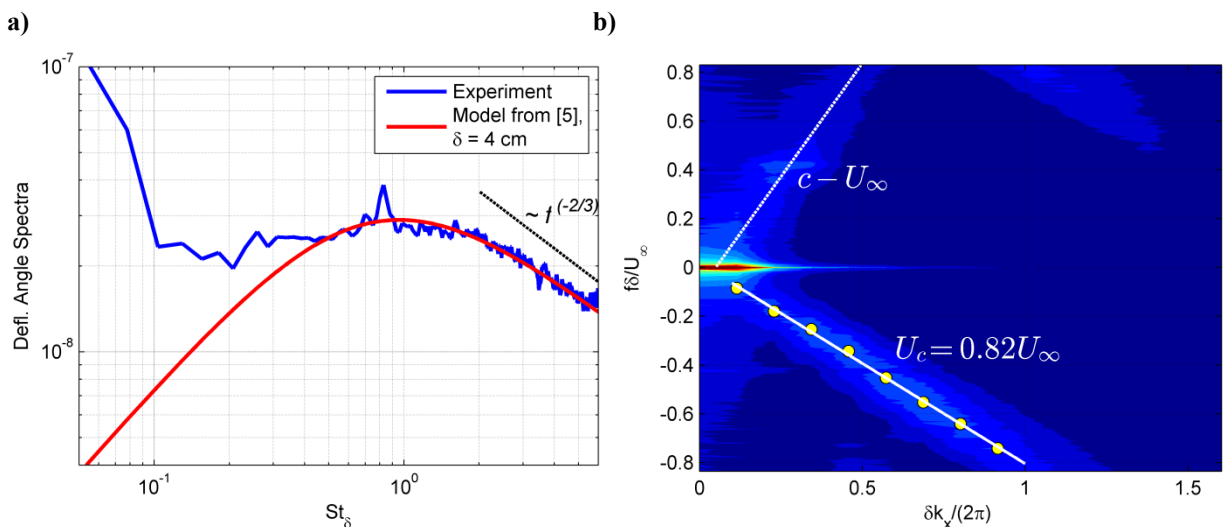


Figure 11. a) Deflection angle spectra from experiment and empirical fit from [5], b) wavenumber-frequency spectra of POD-LSE filtered wavefront data, $M = 0.35$.

Having estimated the boundary layer thickness, the wavenumber-frequency spectrum was computed in the same way as in [5] for the LSE-POD filtered wavefronts, and the results are shown in Figure 11b. By analyzing the slope of various ‘branches’ of the wavenumber-frequency spectrum, the convective speed of aero-optically active portions of the TBL can be measured through the dispersion relation, $f(k_x) = k_x(2\pi)^{-1}U_C(k_x)$, where k_x is the wavenumber in the streamwise direction and U_C is the phase velocity of the travelling wave, which is in general a function of wavenumber [5]. The lower branch of wavenumber-frequency spectra maxima corresponds to waves travelling downstream, and is related to aero-optic effects from the turbulent boundary layer, and as in [5], this group of maxima are linear in wavenumber-frequency space, and has a slope corresponding to a convective velocity of $0.82U_\infty$. In addition to the lower boundary-layer branch of the dispersion curve, two more branches were found in Figure 11b. The horizontal branch at $f = 0$ is related to a stationary aero-optical structure, and the upper branch was found to correspond to travelling waves convecting upstream, and has been observed in prior measurements in this facility [5]. This branch, which corresponds to a convection velocity of approximately $-c + U_\infty$, was found to be the result of acoustic contamination traveling upstream from the fan motor into the test section [5].

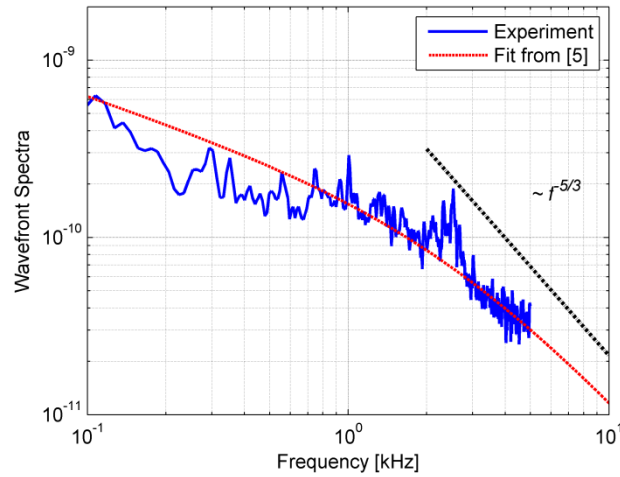


Figure 12. TBL wavefront spectra from experiment and empirical model from [5].

The frequency spectrum of the LSE-POD filtered wavefront was computed and compared to the TBL model from [5] in Figure 12. These results show good agreement with the model wavefront spectra, and the experimental results appear to be approaching the $\sim f^{-(5/3)}$ slope associated with turbulent dissipation in the boundary layer, although it is clear from examining the model fit that the sampling rate of 10 kHz is not high enough to resolve this region of the spectra experimentally.

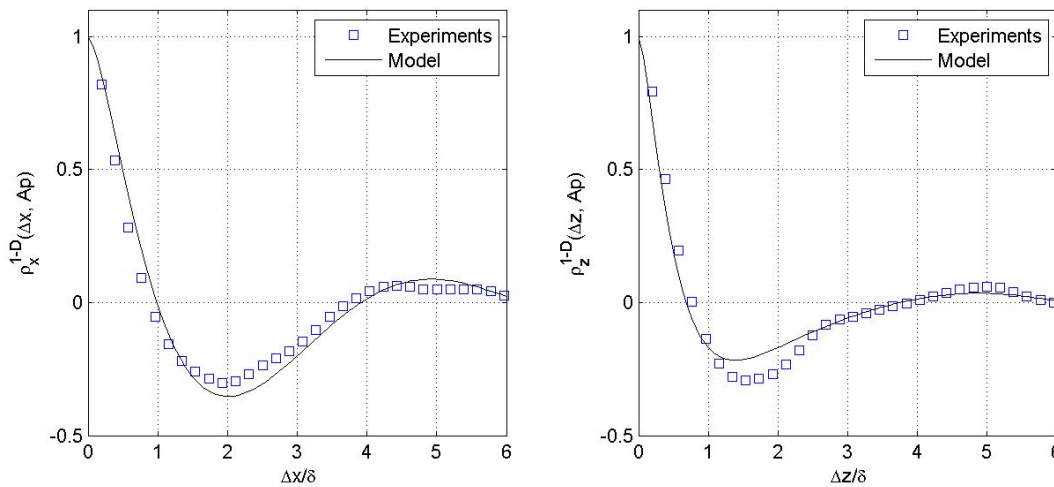


Figure 13. One-dimensional streamwise (left) and spanwise (right) correlations compared with empirical models from [5].

One dimensional streamwise and spanwise correlation functions were computed from the wavefront data by extracting a streamwise slice along the center of each wavefront in the time series (in either the x or z direction, depending on the case). Then, a 1-D autocorrelation was performed on each slice in time, and the result at each instant were averaged to obtain the 1-D correlation function in the x and z directions, which are shown in Figure 13. The experimentally obtained correlation functions show good agreement with models from [5] for streamwise and spanwise spectra. The streamwise correlation length Λ_x , determined from the first minimum location, also shows good agreement with the empirical model and experimental measurements from [5], as seen in Figure 14, left plot. OPD_{RMS} was computed from the LSE-POD filtered data with tip/tilt and piston removed, and the result was normalized by the theoretical value from [5]. This data was plotted against the fit and experimental data presented in [5] in Figure 14, right plot, and is shown to also be in good agreement with previous experimental data and the empirical model from [5].

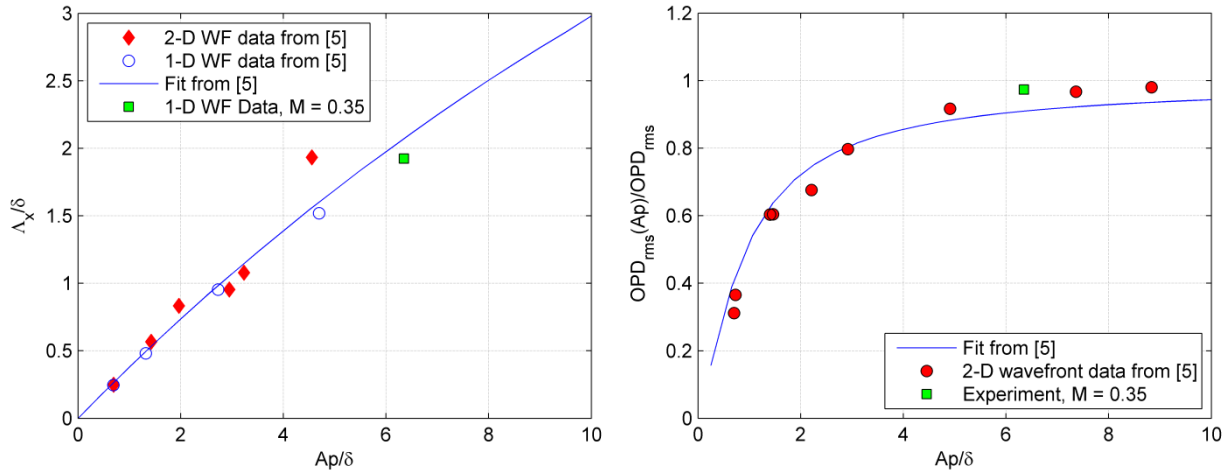


Figure 14. Streamwise correlation lengths (left), defined as a location of the first minimum, and normalized levels of OPD_{RMS} (right) for different streamwise aperture sizes.

V. Conclusions

Wavefront measurements of a turbulent boundary layer were performed at the White Field Tunnel at the University of Notre Dame. Simultaneous accelerometer measurements were performed on the two optical access windows that the laser was propagated through, with up to 16 accelerometers used. Two different accelerometer configurations were used. The data were acquired at $M = 0.25$ and $M = 0.35$.

A combination of POD and LSE were used to isolate the vibration-induced optical aberrations in the wavefronts. First, POD was performed in the spectral domain on the wavefront data, giving the fastest converging modes observed in the wavefronts at each frequency. As vibration effects typically occur at discrete frequencies, usage of POD in the spectral domain converges on the vibration-induced modes at these discrete frequencies rapidly, saving computation time. With the spectral POD modes obtained, the LSE technique was employed in the spectral domain to estimate the POD coefficients at each frequency. Reconstituting the wavefronts using the POD modes and the difference between the computed POD coefficients and the LSE-estimated coefficients gives the residual wavefront error that is not vibrationally induced. A similar technique was demonstrated to be effective in removing a vibrationally-induced component from aero-optical jitter [10].

The first two POD modes were sufficient at describing the aero-optical spectrum at frequencies below 1000 Hz. These frequencies are dominated by vibration effects. There were several distinct peaks in the spectrum that were driven specifically by vibration of the tunnel optical access windows. At higher frequencies, this region is dominated by boundary-layer induced aero-optical effects. These effects take place at scales much smaller than the aperture size and are spatially uncorrelated, so they require substantially more POD modes to fully characterize them. 30 modes were proved sufficient to characterize the wavefronts at frequencies below 2.5 kHz, and with this number of modes, a combination of the LSE-POD filtering and tip/tilt removal showed a reduction in OPD_{RMS} of up to 95%.

A brief optimization study was performed to determine the number of accelerometers needed to filter the vibrational effects from the wavefronts. The LSE-POD filtering technique was performed with subsets of 2, 4 and 8

accelerometers, and the filtered spectra were compared. A monotonic trend was shown that increasing the number of accelerometers increases the effectiveness of the filtering, but there was a marked improvement with even just 2 accelerometers used. As the optical access windows were relatively large, a larger number of accelerometers were necessary to fully characterize the complex spatial vibration modes. With smaller windows, fewer accelerometers will likely be necessary.

Following the application of the LSE-POD technique to aero-optic measurements of the White Field $M = 0.35$ turbulent boundary layer, filtered wavefront statistics were computed and compared to previous experiments and empirical models from [5]. A convective velocity of 0.82 the freestream velocity was measured, which is consistent with previous work. Wavefront spectra were also found to be in good agreement with the empirical model for wavefront frequency spectra from [5], although it is clear from the comparison that the 10 kHz sampling rate was too low to resolve the high end of the wavefront spectra where $W(f) \sim f^{-5/3}$ due to dissipation of turbulence. One-dimensional streamwise and spanwise wavefront correlation functions were also found to be in good agreement with the empirical model from [5], as well as the streamwise correlation length $\Lambda_x(Ap/\delta)$ and the ratio of $OPD_{RMS}(Ap/\delta)$ to the model-predicted level of OPD_{RMS} . These results clearly indicate the utility of LSE-POD filtered wavefront measurements, and their effectiveness at removing non-aero-optic effects from wavefront measurements which have a low signal to noise ratio.

Acknowledgments

This work is supported by the Arnold Engineering Development Complex, SBIR Project FA9101-13-M-0012. The U.S. Government is authorized to reproduce and distribute reprints for governmental purposes notwithstanding any copyright notation thereon.

References

- [1] M. Wang, A. Mani and S. Gordeyev, "Physics and Computation of Aero-Optics", *Annual Review of Fluid Mechanics*, Vol. 44, pp. 299-321, 2012.
- [2] S. Gordeyev and E. Jumper, "Fluid Dynamics and Aero-Optics of Turrets", *Progress in Aerospace Sciences*, **46**, (2010), pp. 388-400.
- [3] N. De Lucca, S. Gordeyev and E.J. Jumper, "In-flight aero-optics of turrets", *Journal of Optical Engineering*, 52(7), 071405, 2013.
- [4] C. Porter, S. Gordeyev, M. Zenk and E. Jumper, "Flight Measurements of the Aero-Optical Environment around a Flat-Windowed Turret", *AIAA Journal*, Vol. 51, No. 6, Jun. 2013, pp. 1394-1403.
- [5] S. Gordeyev, A. E. Smith, J.A. Cress and E.J. Jumper, "Experimental studies of aero-optical properties of subsonic turbulent boundary layers", *Journal of Fluid Mechanics*, **740**, pp. 214-253, 2014.
- [6] A.E. Smith, S. Gordeyev, E.J. Jumper. Recent measurements of aero-optical effects caused by subsonic boundary layers. *Opt. Eng.* **52** (7), 071404, 2013.
- [7] P.E. Morgan and M.R. Visbal., "Hybrid Reynolds-Averaged Navier-Stokes/Large-Eddy Simulation Investigating Control of Flow over a Turret", *Journal of Aircraft*, **49**(6), pp. 1700-1717, 2012.
- [8] Jelic R, Sherer S, Greenyke R, "Simulation of Various Turrets at Subsonic and Transonic Flight Conditions Using OVERFLOW," *J. of Aircraft*, **50**, pp.398-409, 2013.
- [9] K. Wang and M. Wang, "Aero-Optics of Subsonic Turbulent Boundary Layers," *Journal of Fluid Mechanics*, Vol. **696**, pp. 122-151, 2012.
- [10] N. De Lucca, S. Gordeyev and E. Jumper, "The Study of Aero-Optical and Mechanical Jitter for Flat Window Turrets", AIAA Paper 2012-0623.
- [11] Whiteley, MR, Goorskey DJ, and Drye, R, "Aero-Optical Jitter Estimation Using Higher-Order Wavefronts", *Opt. Eng.* **52** (7), 071411, 2013.
- [12] Berkooz, G., Holmes, P., & Lumley, J. L. 1993, "The proper orthogonal decomposition in the analysis of turbulent flows," *Ann. Rev. Fluid Mech.*, **25**, 539-575.
- [13] Holmes, P., Lumley, J. L., & Berkooz, G., 1996, *Turbulence, Coherent Structures, Dynamical Systems and Symmetry*, Cambridge University Press.
- [14] Lumley, J., 1970, *Stochastic Tools in Turbulence*, Academic, New York.
- [15] Gordeyev S.V. and Thomas F.O., "Coherent Structure in the Turbulent Planar Jet. Part 1. Extraction of Proper Orthogonal Decomposition Eigenmodes and Their Self-Similarity", *Journal of Fluid Mechanics*, **414**, pp. 145-194, 2000.
- [16] Adrian, R.J., "On the role of conditional averages in turbulent theory", In: *Turbulence in Liquids: Proceedings of the 4th Biennial Symposium on Turbulence in Liquids*, ed. G. Pateson and J. Zakin, Science Press, Princeton, 1977, pp. 322-33.
- [17] Cress, J.A. 2010 *Optical aberrations caused by coherent structures in a subsonic, compressible, turbulent boundary layer*. Ph.D. Thesis, Univ. of Notre Dame, Notre Dame, IN